J Solid State Electrochem (1999) 3: 361–369

ORIGINAL PAPER

Andrea Schaufuß · Gunther Wittstock

Oxidation of 2-mercaptobenzoxazole in aqueous solution: solid phase formation at glassy carbon electrodes

Received: 21 January 1999 / Accepted: 15 March 1999

Abstract The redox reactions of 2-mercaptobenzoxazole (MBO) have been investigated by cyclic voltammetry at glassy carbon electrodes in aqueous solution. Four anodic and three cathodic processes could be identified. A more detailed analysis of the oxidation processes up to a potential of +0.6 V (SCE) and the corresponding reduction signals showed that the oxidation leads to bis(benzoxazolyl) disulfide (BBOD). Owing to its low solubility, the oxidation product remains at the electrode surface. This product has been identified by *ex situ* FTIR and XPS analysis. During the reduction of BBOD, mainly MBO is formed. The remarkable lower solubility of BBOD in aqueous solutions compared to MBO allows preparation of layers of BBOD *in situ* and to control the amount of deposited BBOD via the MBO solution concentration and electrolysis time. The peak potential and peak shape of the reduction signals change remarkably as the amount of BBOD increases from submonolayer coverage to coverages that correspond to multilayers. The behavior can be explained by assuming an electrochemical conversion of BBOD microcrystals, which are deposited on the electrode surface, if the amount of BBOD formed during the MBO oxidation exceeds one monolayer.

Key words Solid phase voltammetry · Adsorption · Cyclic voltammetry · Flotation collectors

A. Schaufuß · G. Wittstock (✉)
University of Leipzig,
Wilhelm-Ostwald-Institute of Physical
and Theoretical Chemistry,
Linnéstrasse 2, D-04103 Leipzig, Germany
e-mail: wittstoc@rz.uni-leipzig.de,
Fax: +49-341-9736399

Supplementary material Appendix A, B has been deposited in electronic form and can be obtained from http://link.springer.de/link/service/journals/10008/index.htm

Introduction

The electrochemistry of 2-mercaptobenzoxazole (MBO, Fig. 1) and related compounds has been studied at various electrodes. These studies focused (1) on the determination of 2-mercaptobenzothiazole (MBT) concentration, for instance in rubber, where it finds its most important technological application as accelerator in the vulcanization process [1, 2], (2) on the accumulation of heavy metals by complex formation with MBT or 2-mercaptobenzimidazole (MBI) prior to a voltammetric trace determination of heavy metals at modified electrodes [3, 4], and (3) on electroorganic synthesis [5, 6]. Recently, MBO and MBT have been suggested as new collectors in the flotation of metal sulfide ores [7]. They are effective at much lower volume concentration than xanthates used traditionally for this purpose [8] and bind to important minerals like galena (PbS) [9], pyrite (FeS_2) [10], chalcopyrite ($CuFeS_2$) [11], chalcocite (CuS_2) [12], and CdS [13] at neutral pH, while xanthate flotation is carried out under alkaline conditions [14]. Extensive surface spectroscopic investigation using synchrotron radiation-excited photoelectron spectroscopy (SXPS, [15]) confirmed that MBO and MBT form adsorbed layers on minerals with varying thickness and chemical composition. At MBT solution concentrations below 10^{-5} M a chemisorbed monolayer of MBT is formed on those minerals by forming a coordinative bond between the exocyclic sulfur and metal cations at the mineral surface [9]. The participation of the N atom in the bond formation to the metal ion is not clear yet [16, 17]. With increasing collector concentration, organic multilayers of MBT, its disulfide bis(benzothiazolyl) disulfide (BBTD), and possibly its monosulfide are formed [9]. The formation of disulfide from the xanthate-type collectors is considered to be a prerequisite for the flotation of some minerals because only the more hydrophobic disulfides provide enough hydrophobicity [18]. The extent to which disulfides of MBO and MBT are formed varies significantly between

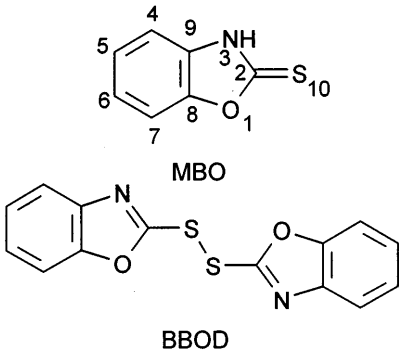

Fig. 1 Structure of MBO and BBOD

different minerals and increases with an increasing band gap in the order PbS < FeS_2 < CdS [19], although this simple scheme does not account for all experimental results.

Although the MBO structure is very similar to that of MBT, MBO chemisorbs to a much lesser extent on all the minerals investigated [19]. The corresponding disulfide [bis(benzoxazolyl) disulfide (BBOD)] is not observed spectroscopically on PbS or FeS_2. In order to separate the role of the semiconducting minerals and the influence of the cations in the adsorption process from the nonspecific hydrophobic interaction of the collectors with surfaces, the electrochemistry of MBT and MBO was also investigated in aqueous electrolytes at glassy carbon (GC) electrodes – a material that, unlike Hg [20] or noble metals [21–23], cannot chemisorb the thiols by metal-sulfur bond formation, while physisorption of the hydrophobic organic molecules can still be expected.

Surprisingly, the behavior of these compounds at GC is all but simple. The unusual dependence of the cyclic voltammograms on scan rate and MBO bulk concentration are explained by the reaction of microcrystals. The latter are formed if a critical amount of collector per electrode area has been oxidized. Microscopic and spectroscopic evidence is presented for the reactions of MBO. The behavior of MBT at GC electrodes will be discussed in a forthcoming paper. Besides the results relevant for flotation research, the study provides an example for the voltammetric behavior of organic microcrystals on electrodes. It is known that cyclic voltammograms (CVs) of substances immobilized onto electrode surfaces by solvent evaporation [24] can exhibit large peak-to-peak separations which are difficult to account for by slow electron transfer in adsorbed layers [25], as the same redox systems show rather rapid kinetics if dissolved in solution. Just recently, the concepts of abrasive stripping voltammetry [26, 27] could explain some of the special features of solid state voltammetry [28] such as the large peak-to-peak separation. These considerations can be extended to organic substances deposited by solvent evaporation onto electrode surfaces, which exhibit a low solubility in the working solution [29]. In the case investigated here, MBO has a limited solubility in the electrolyte but the solubility of the oxidation product is even much lower so that essentially all the oxidation products formed at the electrode will remain at the electrode surface. We demonstrate that if a critical amount of BBOD is formed, the behavior follows that of microcrystals rather than that of an adsorbed layer. In light of the electrochemistry of microcrystals, the MBO study represents a particular interesting example because the microcrystals consist of BBOD whose amount can be adjusted exactly by the solution concentration and the potential program.

Experimental

MBO (95%, Aldrich, Steinheim, Germany) was recrystallized from ethanol. Bis(benzoxazolyl) disulfide (BBOD, Fig. 1) was synthesized by oxidation of MBO with H_2O_2 in cooled acetic acid [30]. Recrystallization from ethanol/water and drying above $CaCl_2$ led to yellow needles. MBO and BBOD identity and purity were characterized by elemental analysis, ^{1}H NMR (400 MHz) and ^{1}H-decoupled ^{13}C NMR, mass spectrometry and melting points. Data are available as Supplementary material. NaH_2PO_4 (Fluka, Buchs, Switzerland), Na_2HPO_4 (Fluka), and ethanol (Roth, Karlsruhe, Germany) were of p.a. quality and used as received to prepare buffers of 0.1 M ionic strength with deionized water (Christ, Stuttgart, Germany, 18 MΩ cm).

Voltammograms were recorded with a PC-controlled Autolab PGSTAT10 (Eco Chemie, Utrecht, Netherlands) with a saturated calomel electrode (SCE, Sensortechnik Meinsberg, Meinsberg Germany) and a coiled Pt wire as counter electrode. All potentials given in this paper are referred to the SCE. Pen-shaped GC disk electrodes (active electrode area 3 mm diameter, total cross section of insulator + active area 6 mm, Bioanalytical Systems BAS, West Lafayette, Ind., USA) were used as working electrodes in the cyclovoltammetric experiments. Experiments that required the transfer of the working electrode into a spectrometer were performed with pieces of glassy carbon (Sigradur G, HTW Hochtemperatur-Werkstoffe, Thierhaupten, Germany) polished in house on a motorized stage on subsequently finer grinding paper and Al_2O_3 slurries for several hours on each corn size (final 0.05 μm). They could be used conveniently as interchangeable electrodes with a holder machined by Senslab (Leipzig, Germany). GC electrodes of both sources gave equivalent CVs of MBO and were cleaned between experiments by polishing 3 min each on Al_2O_3 (0.3 μm and 0.05 μm) on a polishing pad (Buehler, Lake Bluff, Ill., USA) followed by rinsing with water after each polishing step. Surfaces showing reproducible behavior during MBO oxidation were obtained by performing five cyclic voltammograms between −0.8 V and +0.8 V at 0.1 V s^{-1} in the buffer solution used for the following experiment. Buffers were deaerated by bubbling Ar (99.996%, AirLiquide, Düsseldorf, Germany) through the cell for 15 min. During the measurement, Ar was streaming over the liquid surface. Solutions with MBO were prepared with 5% (v/v) absolute ethanol. To allow the establishment of the adsorption equilibrium of MBO, the electrode was held at the starting potential for 120 s.

FTIR spectra were recorded with an IFS 55/S instrument (Bruker, East Milton, Ont., Canada) to which an IR microscope was attached. For adsorbed species, difference spectra are given with the spectrum of polished GC as the background. Reference spectra were obtained by evaporation of 10 μl of a 10^{-2} M solution of the compound in $CHCl_3$ on a NaCl crystal. In these cases the background is the spectrum of the clean NaCl crystal.

Photoelectron spectra were recorded with an ESCALAB 220iXL (VG, East Grinstead, UK) with monochromatized Al K_α excitation. The energy scale of the spectrometer is routinely calibrated by the binding energy of the Au $4f_{7/2}$ (84.00 eV) and Cu $2p_{3/2}$ (932.67 eV) emissions [31]. With a pass energy of 10 eV used for recording single line spectra, the full width at half maxi-

mum is 0.48 eV for the Ag $3d_{5/2}$ signal. The binding energies for modified GC electrodes are given with respect to the graphitic carbon signal of the GC electrode at 284.4 eV. No sample charging was observed for modified GC electrodes. Sample charging encountered during measurement of reference samples (insulating powders) were compensated with an electron flood gun at 4 eV and 0.1 mA emission current. Those signals are given with respect to the C 1*s* line of ubiquitous organic contamination (-CH_2-) at 284.7 eV. Interpretation of spectra was facilitated by the program UNIFIT for Windows [32], which allows very convenient least square fitting of the experimental spectra by a Shirley-type background [33] and several spectral components. The special advantage of that program is the possibility to describe the peak as a true convolution of Gaussian and Lorentzian contributions, whereas most other packages use the simplifying multiplication of Gaussian and Lorentzian contributions. Background-subtracted experimental data are given as solid circles, individual components and the sum of all components are represented as solid lines.

Results and discussion

Voltammetric signals for MBO oxidation

Typical cyclic voltammograms of MBO are shown in Fig. 2. Four anodic processes labeled Ia through IVa can be identified. By systematically varying the anodic switching potential E_λ it can be shown that the cathodic process Ic (−0.09 V) corresponds to the anodic process Ia at +0.14 V (Fig. 2, curve 1). It is a conversion of an adsorbed product because the current decreases to zero after passing through the peak. The peak Ic is not observed if E_λ is more positive than the second oxidation process IIa at +0.36 V (Fig. 2, curves 2–4). In this case the cathodic peak IIc (−0.46 V) develops. The inset compares the total cathodic and anodic charges passed in one cycle. From this graph it is evident that up to E_λ = +0.8 V the cathodic charge is exactly equal to the anodic charge. This observation is independent from the scan rate in the concentration range investigated (0.2–5 mM), leading to the conclusion that *all* the products formed during the oxidation remain at the electrode and are available for the reduction in the second half-cycle. Deviation from this behavior is seen if E_λ is more positive than peaks IIIa (+0.84 V) and IVa (+1.20 V), causing development of another cathodic signal IIIc (−0.7 V). In this paper we restrict the discussion to the processes occurring up to a potential of +0.8 V. The signals IIIa, IVa, and IIIc are caused by a rather complicated mechanism leading to the formation of a polymer film during multi-cycle experiments. They are observed more clearly in solution of low MBO bulk concentration when signal IIa is diminished. Under these condition, signal IIIc is not observed. As the investigation of these reactions by cyclic voltammetry, microscopy, FTIR, XPS, and SIMS would divert from the focus of this paper, details will be reported separately.

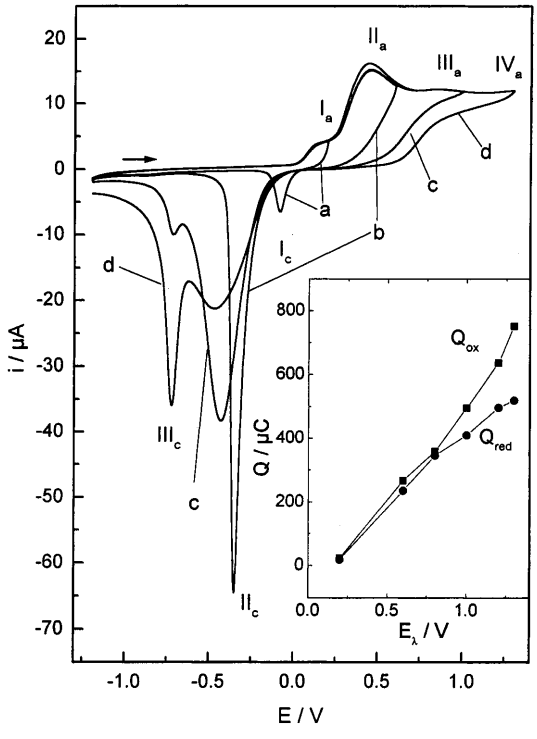

Fig. 2 Cyclic voltammograms of 3 mM MBO in phosphate buffer (pH 7) at 0.025 V s^{-1} scan rate with various anodic switching potentials E_λ. Anodic and cathodic peaks are labelled for discussion in the text. *Inset*: Anodic (■) and cathodic (●) charges as a function E_λ

It is instructive to arrange the CVs of MBO obtained with E_λ = +0.8 V and a range of scan rates and MBO bulk concentrations as a matrix (Fig. 3). There are two distinct types of CV within this set. Process IIa is more important at high MBO bulk concentration *c*(MBO) and low scan rates *v* (Fig. 3a, b, e, f), whereas process Ia dominates the CVs at low *c*(MBO) and high *v* (Fig. 3l, o, p). This feature suggests that signal Ia results from the oxidation of an adsorbed species, while signal IIa is caused by the oxidation of a diffusing reactant. This assumption can be verified by several criteria. The peak current for signal Ia is proportional to the scan rate (Fig. 4a), indicative of an immobilized redox system. It was determined as the difference to the extrapolated background current. Peak currents for peak IIa were approximated as the difference of the peak current measured against the same baseline and the peak current of signal Ia. The peak current for signal IIa follows a proportionality to the square root of scan rate (Fig. 4b), typical for diffusion-controlled reactions. Therefore, the contribution of this signal dominates the CV as lower *v* are used. Further evidence comes from the dependence of the peak currents on *c*(MBO) at constant scan rate (Fig. 5). As expected for the reaction of adsorbed species, signal Ia approaches a saturation value at high *c*(MBO) while signal IIa increases proportionally with *c*(MBO). If experiments are performed during turbulent stirring, the signal IIa is enhanced and shows increased noise and increased currents due to convection of the solution, indicating that it represents a diffusion-controlled process (Supplementary material). Signal Ia is unchanged, as expected for the oxidation of a previously

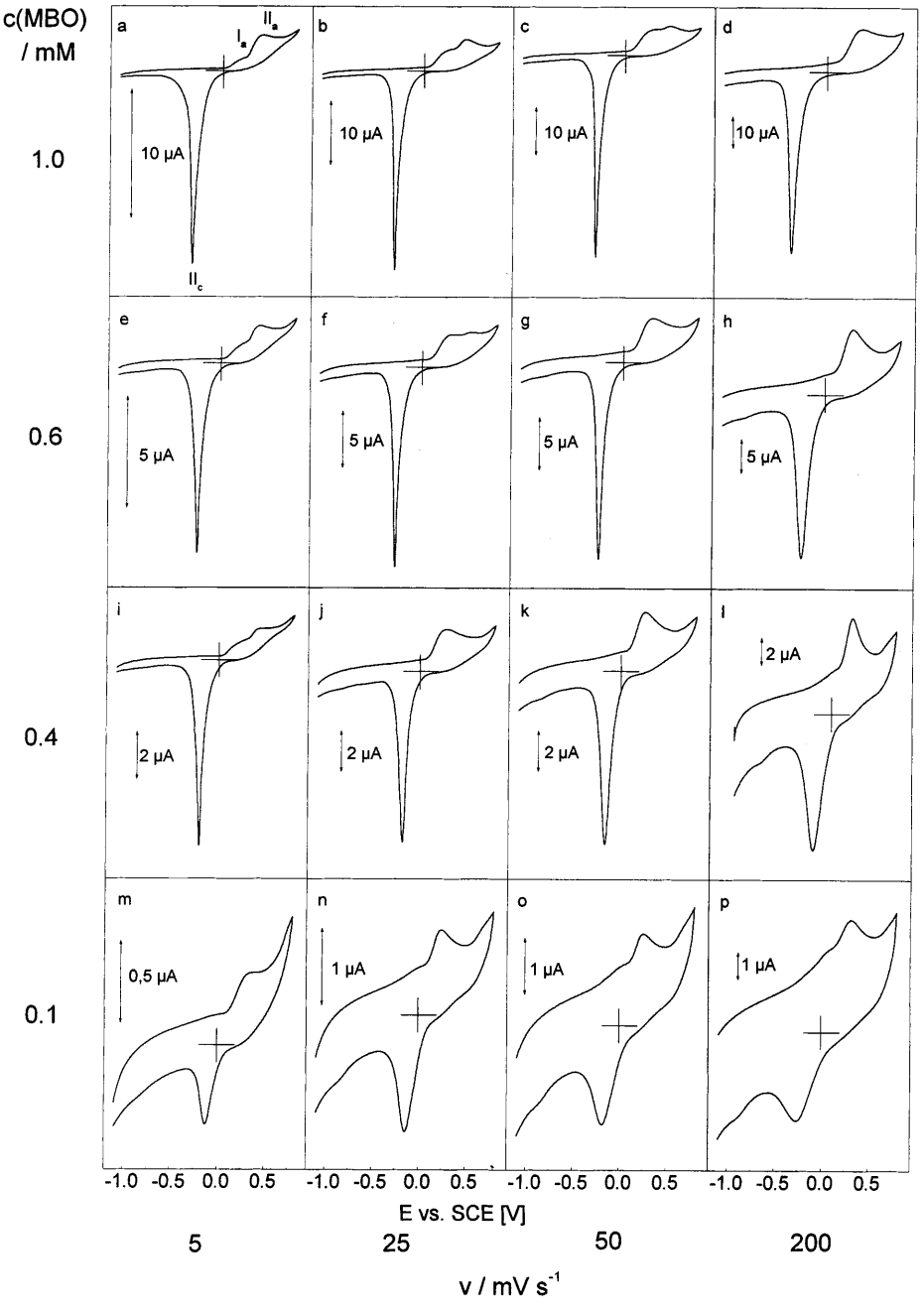

Fig. 3 Cyclic voltammograms of MBO in phosphate buffer (pH 7); scan rates v and MBO bulk concentrations c(MBO) are given at *bottom* and *left margins*; current scales are given for each CV separately

adsorbed species. The cathodic signal IIc is enhanced but does not show increased noise due to convection. This signal will be discussed in detail below. The peak potential for signal Ia is not dependent on c(MBO). The peak potential for signal IIa decreases as c(MBO) increases, and increases as the sweep rate v increases. This is in qualitative agreement with earlier reports on dimerization reactions by Savéant and Vianello [34]. They used the slope of E_p versus log(c) and E_p versus log(v) plots as diagnostic criteria for dimerization mechanisms where both reactants and products are dissolved. The utilization of these criteria in a quantitative way is prevented by the limited concentration and sweep rate ranges under which signal IIa could be observed, the limited accuracy of peak potential determination under the condition of a partially overlapping pre-peak, and the unknown influence of adsorbed reactant and product layers on the kinetics and possible mechanisms of the dimerization.

According to the literature, oxidation of MBO, MBT, and MBI may lead to the corresponding disulfides [6, 35, 36], monosulfides and elemental sulfur [5], or sulfonic acids [37] under different experimental conditions. In analogy to recent results on related compounds, polysulfides [38] can be expected. It is shown here that the disulfide is the dominant oxidation product in aqueous solution at a GC electrodes up to $E = +0.8$ V.

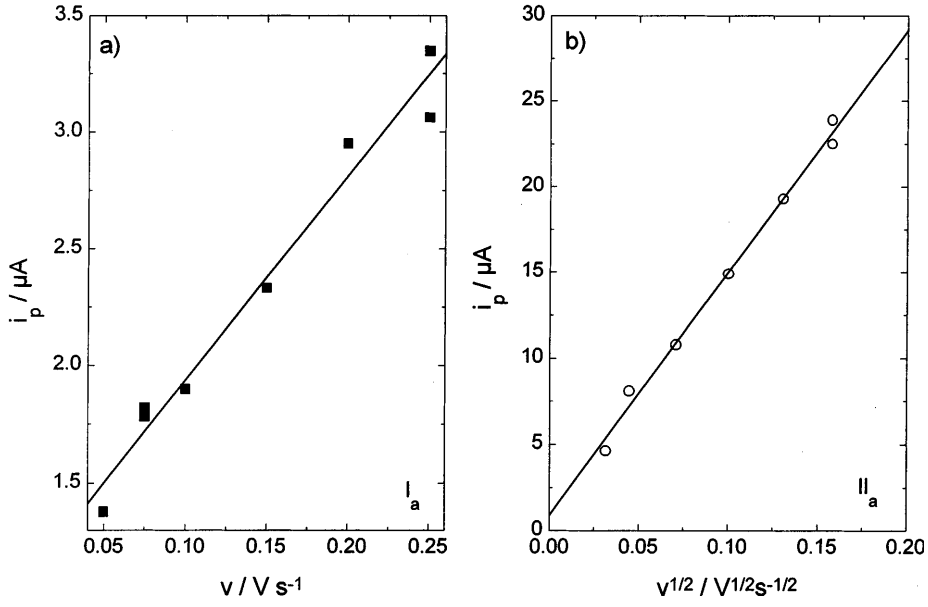

Fig. 4 Dependence of peak currents for signal Ia and IIa from scan rate; **a** peak current of process Ia vs. scan rate; c(MBO) = 0.2 mM; **b** peak current of process IIa vs. square-root of scan rate; c(MBO) = 5 mM

As discussed above, all the products of processes Ia and IIa remain at the electrode surface up to a switching potential E_λ = +0.8 V (Fig. 2, inset). In particular, a sulfonic acid is unlikely as the oxidation product because its solubility in aqueous solution is higher than that of MBO and it would be expected to desorb easily from the electrode. Because the oxidation products are attached to the electrode surface, their chemical nature can be determined by spectroscopic techniques after immersion of the electrode. Having confirmed the chemical nature of the oxidation product, the influence of the amount of oxidation product on the reduction signal IIc is studied and the influence on microcrystallinity is discussed.

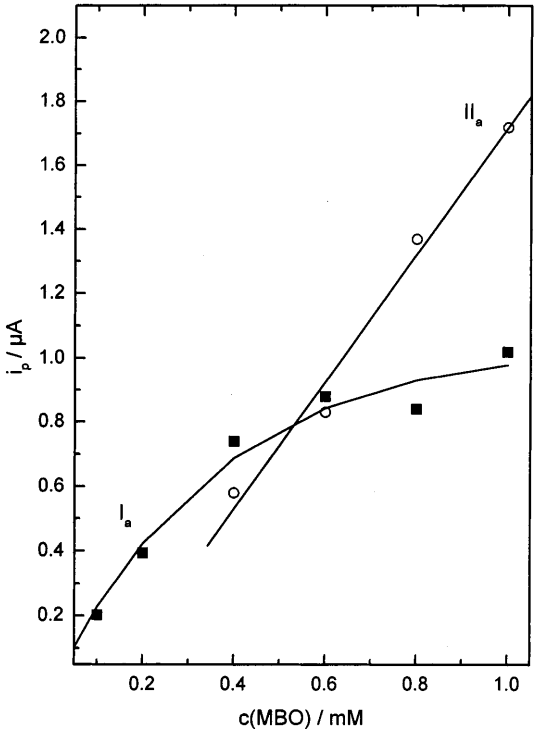

Fig. 5 Dependence of peak currents for signal Ia (■) and IIa (○) on MBO bulk concentration; pH 7, v = 0.005 V s^{-1}. *Solid lines* are spline interpolations to highlight the trend in the data set

Spectroscopic identification of MBO oxidation product

Comparison of the FTIR spectra of chemically synthesized BBOD and the oxidation product on the GC electrode (Fig. 6) demonstrates that BBOD is indeed the product formed during the electrochemical oxidation. Because all bands found at the electrodes immersed at +0.6 V (after process IIa) are matched by those of pure BBOD, it is clear that there are no other oxidation products at comparable amounts. Up to +0.6 V (SCE) the oxidation proceeds according to

$$2\mathrm{MBO} \rightleftharpoons \mathrm{BBOD} + 2\mathrm{e}^- + 2\mathrm{H}^+.$$

Static secondary ion mass spectrometry does not provide additional information under the experimental conditions available to us, because BBOD and other possible oxidation products are volatile at room temperature in ultra-high vacuum (UHV). XPS spectra of immersed GC electrodes could be measured at 200 K and at room temperature (298 K). The cooled GC electrodes show a very intensive S 2$p_{3/2}$ signal at 164.4 eV and a N 1s signal at 399.0 eV (Fig. 7). They are matched by the signals of chemically synthesized BBOD. Sublimation of BBOD in UHV at room temperature results in greatly diminished intensities of the signals of BBOD. The loss of signal intensity corrected by the instrumental sensitivity factors for the S 2p and N 1s emissions has a ratio of 1:1, corresponding to the atomic ratio S:N in BBOD. The N 1s signal of the modified GC electrodes at 400.0 eV originates from the GC electrode itself. A rest

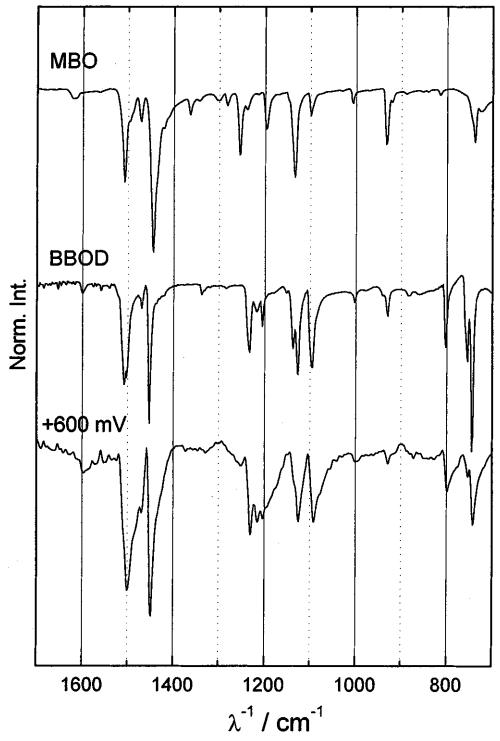

Fig. 6 *Ex situ* FTIR difference spectra of GC electrodes after potential scans from −1.2 V in 3 mM MBO solution at pH 7 up to the indicated emersion potential; background is the spectrum of polished and electrochemical pretreated GC. Spectra of BBOD and MBO are given as reference

remains on the warmed-up electrode, showing S $2p_{3/2}$ and N 1*s* binding energies of 161.9 and 164.2 eV and 399.0 eV, respectively. These peaks become the dominant signal if continuous potential cycling is extended beyond $E_\lambda = +0.8$ V, where the formation of a polymer occurs. Most likely the signals result from initial stages of the polymer film formation and will be dicussed in detail with other experiments on that problem.

Reduction of BBOD

Further evidence consistent with the spectroscopic results can be obtained if chemically synthesized BBOD is dissolved in $CHCl_3$ and deposited onto a rotating GC electrode. After evaporation of the solvent, a CV of the modified electrode is recorded in aqueous phosphate buffer (pH 7), where BBOD is almost insoluble. A reduction is observed at −0.2 V (Fig. 8a). The reduction product is mainly MBO but considerable amounts of byproducts are formed. Because MBO and other possible reduction products are slightly soluble in the electrolyte, they diffuse away from the electrode. Therefore, only a small oxidation signal at +0.3 V is observed in the subsequent positive-going half-cycle (Fig. 8b).

BBOD decomposes slowly (over months) if stored as powder under air. The decomposition products are MBO and benzoxazolinone, as identified by IR spectroscopy. If old batches of chemically synthesized

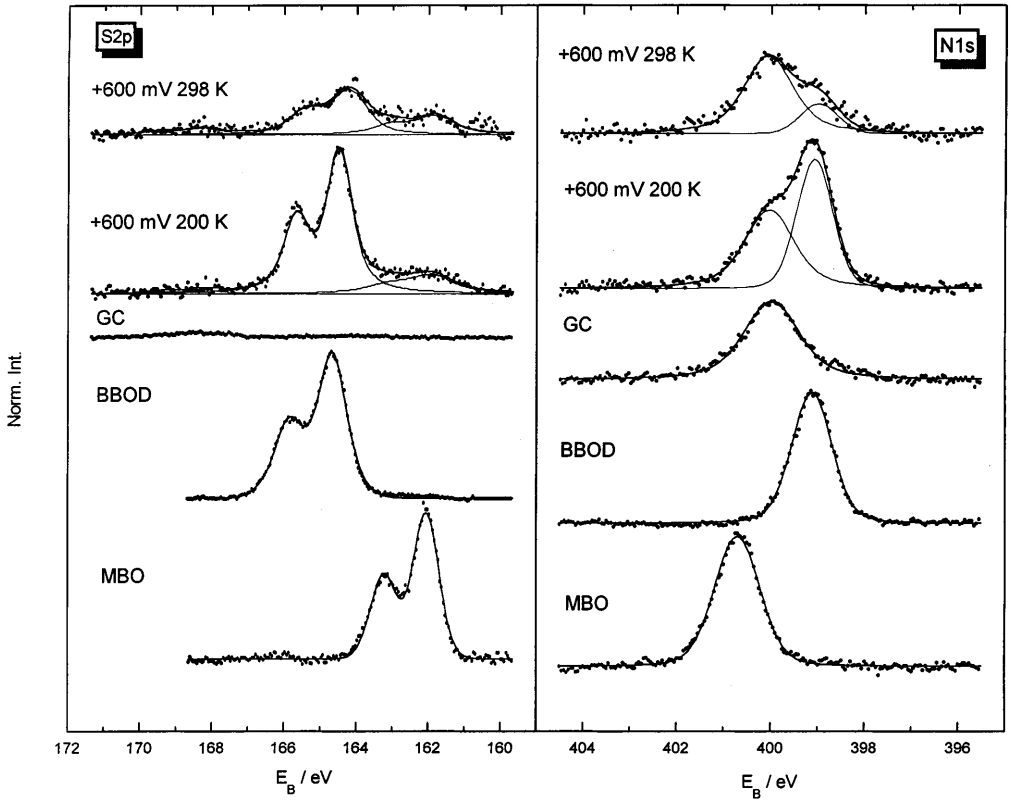

Fig. 7 XPS spectra of the N1*s* and S 2*p* region of GC electrodes emmersed at the indicated potential after a potential scan starting at −1.2 V in 0.5 mM MBO solution (pH 7). For comparison, spectra of a polished GC electrode as well as of MBO and BBOD powders are given below

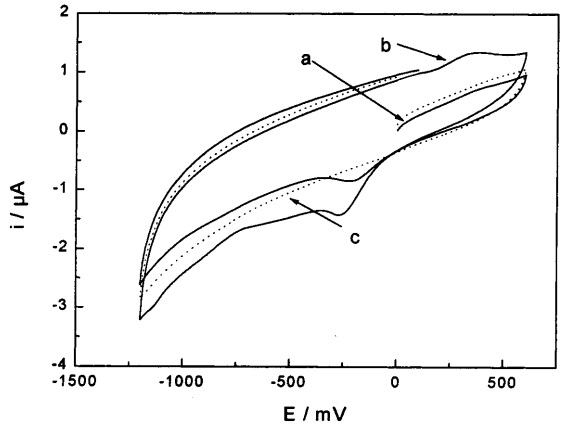

Fig. 8 Cyclic voltammograms of spin-coated BBOD on GC in phosphate buffer (pH 7) with $v = 0.025$ V s^{-1}: *a* first cycle, *b* second cycle. The CV of blank GC is given for comparison *c*

BBOD are deposited on GC, we observe a small oxidation signal at +0.4 V in the initial positive-going scan. This signal increases with the storage time of BBOD.

Electroreduction of electrochemically formed BBOD

A careful inspection of the reduction peaks IIc in Fig. 3 reveals interesting details. The peak width $w_{1/2}$, given as full width at half maximum, decreases, from 281 mV in Fig. 3p (0.2 V s^{-1}, 0.1 mM MBO) to 58 mV in Fig. 3a (0.005 V s^{-1}, 1 mM MBO). As outlined by the compilation of cathodic charges (Table 1) and $w_{1/2}$ (Table 2) for all CVs shown in Fig. 3, $w_{1/2}$ decreases with increasing c(MBO) for a given v. Increasing the bulk concentration of MBO leads to a higher amount of BBOD deposited on the electrode. Lavrion [39, 40] showed for the special case of Frumkin-type adsorption, where the reduced and oxidized reactants R and O replace the same number ν of solvent clusters, that $w_{1/2}$ is controlled by a parameter $x = \nu(a_{RR} + a_{OO} - 2a_{RO}) \times \theta_T$. In this notation, a_{RR}, a_{OO}, and a_{RO} are the interaction coefficients for interactions between R-R, O-O, and R-O, respectively; θ_T represents the sum of coverage of R and O. If there is attractive interaction ($a > 0$) for O-O and R-R or a repulsion for R-O ($a_{OR} < 0$), x will increase with θ_T. If $x \geq 2$, the peak shape cannot be defined mathematically. Lavrion [40] provides a very instructive reasoning and physical interpretation of this fact. A qualitative similar situation may be expected in our case. There are, however, important differences. Experimental verifications for the theory of Lavrion have been obtained using mercury electrodes [39], where uniform adsorption sites can be assumed. Solid electrode surfaces such as GC possess non-equivalent adsorption sites. Therefore the adsorption process cannot be described by a Frumkin isotherm. On such electrodes, peak broadening has been observed with increasing surface concentration and was related to kinetic dispersion [25] caused by the different microenvironments of the adsorbed reactants. As shown below, the amount of BBOD present at the electrode surface corresponds to multilayers. As the amount of BBOD increases, the peak potentials are shifted by about 0.2 V, in contrast to some 10 mV predicted for the case of Frumkin adsorption with strong intermolecular attraction [40].

Assuming an unordered monolayer of BBOD ($M = 300$ g mol^{-1}) having the same density ρ as the solid powder (1.43 g cm^{-3}), one obtains an area density $(\rho/M)^{2/3}$ of 3.32×10^{-10} mol cm^{-2}. Assuming a roughness factor $r = 1$ [41] for the glassy carbon electrode ($A = 0.07$ cm^2) and a two-electron reduction, the charge required to reduce a monolayer of BBOD is 4.5 µC. Assuming an oriented adsorption with the ring system perpendicular to the electrode surface results in a charge of 12.4 µC. All CVs having a reduction charge of this magnitude are highlighted by a bold box in Tables 1 and 2. If the charges exceed this value, $w_{1/2}$ decreases proportional to the logarithm of the cathodic charge, which is proportional to the amount of BBOD on the electrode surface (Fig. 9). If the cathodic charge is larger than 37 µC, $w_{1/2}$ remains approximately constant at 65 mV. The scattering around this value for $Q_{red} > 37$ µC is probably also caused by the different scan rates used to record the data points in this section of the plot. The constant small peak width at higher Q_{red} reflects the situation where BBOD is present at the electrode surface as microcrystals only. The decrease of $w_{1/2}$ for the Q_{red} values corresponding to submonolayer coverage up to 37 µC can be described as superposition of reduction from adsorbed layers and microcrystals present at other parts of the surface.

Table 1 Cathodic charges of the peaks IIc of Fig. 3 The values highlighted by a bold box correspond to a coverage up to one monolayer (see text)

c(MBO) (mM)	Q_{red} (µC) v (V s^{-1})			
	0.005	0.025	0.05	0.2
1	347	109	72	33
0.6	185	65	37	24
0.4	151	37	22	10
0.1	13	11	6	3

Table 2 Peak width ($w_{1/2}$) of the reduction peaks IIc in Fig. 3. The values highlighted by a bold box correspond to a coverage up to one monolayer (see text)

c(MBO) (mM)	$w_{1/2}$ (mV) v (V s^{-1})			
	0.005	0.025	0.05	0.2
1	58	61	58	93
0.6	77	63	75	135
0.4	73	100	117	190
0.1	110	176	195	281

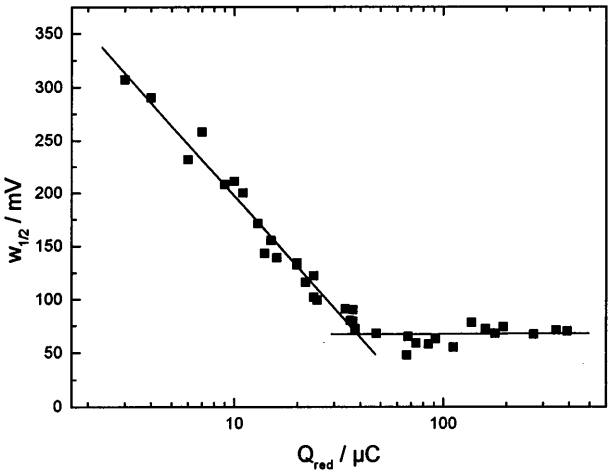

Fig. 9 $w_{1/2}$ of the cathodic peak as a function of the cathodic charges for CV between −1.2 V and +0.8 V for all combinations between scan rates (in V s^{-1}) of 0.005, 0.01, 0.025, 0.05, 0.1, 0.2, and *c*(MBO) (in mM) of 0.1, 0.2, 0.4, 0.6, 0.8, 1.0 (■). *Solid lines* obtained by a fit for $Q_{red} < 37$ µC and $Q_{red} > 37$ µC serve to highlight the trend of the data

Besides peak width, the general peak shape also changes. The inflection points move very close to the peak potential, giving the peak a very pointy appearance. Such peaks are typical for processes that are limited by phase formation phenomena, as in the reaction of microcrystals. The coincidence of peak shapes typical for microcrystals, with the Q_{red} exceeding the charge expected for a reduction of a monolayer, confirms the conclusion that microcrystals start to form if the coverage is higher than about one monolayer. This is reasonable, as the formation of a compact microcrystal can only be envisioned if there is an interaction between neighboring BBOD molecules deposited on the electrode surface. There is a much lower chance of such interaction at submonolayer coverage and the molecules behave as an adsorbed layer.

Recently, Komorsky-Lovric [42] observed a shift of 0.300 V towards more negative potentials for the reduction of azobenzene microcrystals on graphite versus reduction of azobenzene adsorbed from solution. This additional indication is also evident for the reduction of BBOD. The cathodic peak potentials IIc shift to more negative values at constant *v* if the amount of BBOD formed at the electrode during the positive-going half cycle increases at higher MBO solution concentrations (Table 3).

Finally, optical microphotographs of the BBOD microcrystals could be obtained (Fig. 10). The formation of a dendritic solid deposit with micrometer extensions can clearly be seen. This deposit dissolves to a large extent at the negative-going scan. As indicated by the XPS spectra (Fig. 7, top), the rest represents most likely initial stages of a polymer film formation becoming more prominent during multi-cycle experiments with $E_\lambda > +0.8$ V.

Table 3 Dependence of the reduction peak potential IIc on the MBO solution concentration at $v = 0.005$ V s^{-1}

c(MBO) (mM)	0.1	0.2	0.4	0.6	0.8	1.0
E_p (V)	−0.123	−0.141	−0.204	−0.248	−0.313	−0.319

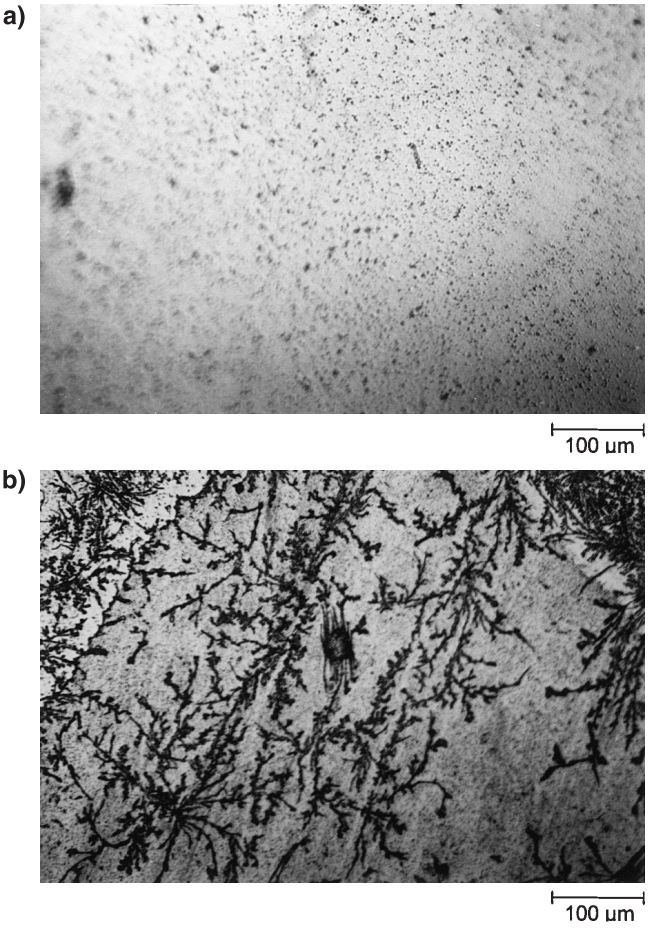

Fig. 10 Interference microphotographs of a GC electrode after polishing (**a**) and after a potential scan from −1.2 V to +1.3 V at 0.025 V s^{-1} in 3 mM MBO solution at pH 7 (**b**)

Conclusion

MBO can be oxidized at GC. Four oxidation signals can be identified. The first two signals are caused by the oxidation of adsorbed and diffusing MBO, respectively. Up to a potential of +0.8 V, BBOD is the dominant oxidation product. The significantly lower solubility of BBOD in aqueous solutions compared to MBO allows preparation of layers of BBOD *in situ* and to control the amount of deposited BBOD via MBO solution concentration and electrolysis time. Peak potential and peak shape of the reduction signals change remarkably as the amount of BBOD increases from submonolayer coverage to coverages that correspond to multilayers. The

behavior can be explained by assuming an electrochemical reduction of BBOD microcrystals which are formed on the electrode surface if the amount of BBOD present at the electrode surface exceeds one or a few monolayers.

Acknowledgement The authors thank V. Gottschalch (University of Leipzig) for providing access to the interference microscope. FTIR spectra were recorded during a stay of A.S. in the group of G.M. Bancroft (University of Western Ontario) and at Surface Science Western with technical assistance of N.S. McIntrye, M.J. Walzac, and B. Berno. A.S. received grants from the German National Scholarship foundation and from the Graduate Course Physical Chemistry at Surface and Interfaces at the W.-Ostwald-Institute funded by Deutsche Forschungsgemeinschaft. Investigation of MBO as a flotation collector was funded by Deutsche Forschungsgemeinschaft under grant Sz 58/4–1 to R. Szargan, to whom we are in debt for continuous encouragement to pursue this facet of the overall project goals.

References

1. Scholz F, Kreutzmann A, Lange B, Dietzsch T, Henrion G (1989) Z Chem 29: 216
2. Fogg AG, Ismail A, Ahmad R, Banica FG (1997) Talanta 44: 491
3. Sousa MF, Bertazzoli R (1996) Anal Chem 68: 1258
4. Khan MM, Khoo SB (1996) Anal Chem 68: 3290
5. Chambers JQ, Moses PR, Shelton RN, Coffen DL (1972) J Electroanal Chem 38: 245
6. Chandrasekaran M, Krishan V (1986) Trans SAEST 21: 25
7. Cozza C, Di Castro V, Polzonetti G, Marabini AM (1992) Int J Miner Process 34: 23
8. Maier G, Qiu X, Dobiás B (1997) Colloids Surf 10: 1375
9. Szargan R, Uhlig I, Wittstock G, Roßbach P (1997) Int J Miner Process 51: 151
10. Schaufuß A, Roßbach P, Uhlig I, Szargan R (1997) Fresenius J Anal Chem 358: 262
11. Numata Y, Wakamatsu T (1994) In: Sohn Y (ed) Metallurgical processes for the early 21st century, vol 1. The Mineral, Metals & Materials Society, Warrendale, PA p 1015
12. Contini G, Laajalehto K, Suoninen E, Marabini AM (1995) Surf Interface Anal 17: 234
13. Mayer D, Hallmeier KH, Chassé T, Szargan R (1998) Fresenius J Anal Chem 361: 689
14. Fuerstenau MC, Miller JD, Kuhn MC (1985) Chemistry of flotation. American Institute of Mining, Metallurgical and Petroleum Engineers, New York, p 33
15. Szargan R, Uhlig I, Wittstock G (1998) Surf Invest 13: 499
16. Banerji S, Byrne RE, Livingstone SE (1982) Trans Met Chem 7: 5
17. Yoshida T, Yamasaki K, Sawada S (1979) 52: 2908
18. Karthe S, Szargan R, Suoninen E (1993) Appl Surf Sci 72: 157
19. Szargan R, Schaufuß A, Roßbach P (1999) J Electron Spectrosc Rel Phenom (in press)
20. Sartori G, Liberti A (1950) J Electrochem Soc 97: 20
21. Zerulla D, Uhlig I, Szargan R, Chassé T (1998) Surf Sci 404: 604
22. Xue G, Lu Y (1994) Langmuir 10: 967
23. Marconato JC, Buhoes LO, Temperini ML (1998) Electrochim Acta 43: 771
24. Takehara K, Ide Y (1991) Bioelectrochem Bioenergetics 26: 297
25. Honeychurch JM, Rechnitz GA (1998) Electroanalysis 10: 453
26. Scholz F, Meyer B (1994) Chem Soc Rev 23: 341
27. Lovric M, Scholz F (1997) J Solid State Electrochem 1: 108
28. Scholz F, Lovric M, Stojek Z (1997) J Solid State Electrochem 1: 134
29. Shaw SJ, Marken F (1996) Electroanalysis 8: 732
30. Arbuzov BA, Zoroastrova (1959) Izv Akad Nauk Otd Khim 6: 1037
31. Seah MP (1989) Surf Interf Anal 14: 488
32. Hesse R, Chassé T, Szargan R (1999) Fresenius J Anal Chem (in press)
33. Seah MP (1990) In: Briggs D, Seah MP (eds) Practical surface analysis, vol 1, 2nd edn. Salle + Sauerländer, Frankfurt, pp 233–240
34. Savéant JM, Vianello E (1967) Electrochim Acta 12: 1545
35. Goyal RN, Kumar A (1992) Indian J Chem 31 A: 237
36. Goyal RN, Verma MS (1996) Indian J Chem 35 A: 281
37. Skacel P, Karlik M, Kucera Z, Dolezal B (1985) Sci Pap Prague Inst Chem Techn H20: 31
38. Le Guillanton G, Do QT, Elothmani D (1996) J Electrochem Soc 143: L223
39. Lavrion E (1982) In: Bard AJ (ed) Electroanalytical chemistry, vol 12. Dekker, New York, pp 53–157
40. Lavrion E (1975) J Electroanal Chem 63: 245
41. Thornton DC, Corby KT, Spendel VA, Jordan J, Robbat A, Rustrom DJ, Gross M, Ritzler G (1985) Anal Chem 57: 150
42. Komorsky-Lovric S (1997) J Solid State Electrochem 1: 94